Deciphering the Synergy Between Plasma and Catalyst Support for Ammonia Synthesis in a Packed DBD Reactor

Bhaskar S. Patil[a*], Floran J. J. Peeters[b], Alwin S. R. van Kaathoven[a], Jürgen Lang[c], Qi Wang[a], Volker Hessel[a*]

[a]Laboratory of Chemical Reactor Engineering / Micro Flow Chemistry and Process Technology, Department of Chemical Engineering and Chemistry, Eindhoven University of Technology, P.O. Box 513, 5600 MB Eindhoven, The Netherlands

[b]Dutch Institute for Fundamental Energy Research (DIFFER), P.O. Box 6336, 6500 HH Eindhoven, The Netherlands.

[c]Innovation Management, Verfahrenstechnik & Engineering, Evonik Industries AG, Rodenbacher Chaussee 4, 63457 Hanau-Wolfgang, Germany.

[*]corresponding authors: *Volker Hessel,* email: V.Hessel@tue.nl , telephone: +31(0)40 247 2973 and *Bhaskar S. Patil* at Bhaskar_Patil@outlook.com

ABSTRACT

Plasma-assisted ammonia synthesis in a packed Dielectric Barrier Discharge (DBD) reactor at atmospheric pressure is presented in this work. A broad range of materials (commonly used as catalyst supports) with various chemical properties (acidic α-Al_2O_3, TiO_2 and basic MgO, CaO), surface area and porosity (α-Al_2O_3 and γ-Al_2O_3), dielectric properties (quartz wool, TiO_2, and $BaTiO_3$), have been investigated for synergetic effects by packing them in the discharge zone of the DBD reactor. All the materials showed a substantial effect on ammonia production. Dielectric properties, size and shape of packing material are found to be the key parameters to enhance plasma. Quartz wool, followed by γ-Al_2O_3, produce the highest concentration of ammonia at 2900 and 2700 ppm, respectively, due to their ability to generate dense filamentary microdischarges. Particles 200 µm in diameter of yielded a 64% higher concentration of NH_3 than 1300 µm particles – because of amplified electric field strength from increased particle-particle contact points. The specific energy input per unit volume has a significant impact on the ammonia production. The process parameters such as a N_2/H_2 feed flow ratio, total flow rate and argon dilution have also been investigated. The N_2/H_2 feed flow ratio above 2 increase ammonia concentration and energy efficiency compared to the stoichiometric ratio of 0.33. At 0.4 L min^{-1}, 3500 ppm of ammonia was produced with an energy efficiency of 1.23 g NH_3 kWh^{-1}. Dilution with 2-5 vol% of argon yields 2% improvement in the concentration and energy efficiency, which seems insignificant considering the added practical challenges posed by gas separation.

KEYWORDS: Plasma-assisted ammonia synthesis; DBD reactor; catalyst supports; support size; synergy.

1 INTRODUCTION

Ammonia, being the second largest produced chemical compound by volume with vital for economy and society [1,2]. Ammonia is irreplaceable in fertilizer production which sustain 40% of the global population [3]. Moreover, ammonia is also used as a starting compound to produce chemicals such as polyamides, Ɛ-caprolactam, hydrazine and explosives. All the ammonia is produced by the Haber-Bosch process – the process developed in the beginning of the 20th century that combines nitrogen with hydrogen at 450-600^{o}C and 150-350 bar in the presence of a catalyst [4]. The process consumes more than 1% of the world energy and emits around 300 million metric tons of CO_2 [5,6].

Modern technological and ecological demands create new niches for ammonia such as in NO_x abatement from diesel engines by selective catalytic reduction [7] and as an energy storage chemical [8,9]. These new developments demand localized small-scale ammonia production, for which the Haber-Bosch process is suitable technically or economically.

One of the most promising possibilities to produce ammonia at a small scale is the synthesis with non-thermal plasma driven by renewable electricity [10–16]. In this plasma, the temperature of electrons is high (1-10 eV) and the bulk of the gas remains at low temperature [17,18]. This non-equilibrium nature enables thermodynamically unfavourable reactions such as ammonia formation at an atmospheric pressure and lower temperatures.

Non-thermal plasma can be combined with heterogeneous catalysis to increase the reaction yield and selectivity [19–21]. Combining plasma and catalyst often leads to a synergetic effect – the effect where the production of ammonia produced in plasma-catalysis exceeds the expected sum of effects of plasma and catalysis separately. This synergy could arise from the enhancement of plasma by the catalyst materials or chemical interactions between the activated plasma species and catalysts [22,23].

Plasma-assisted synthesis of ammonia has been investigated using various types of non-thermal plasma: glow [24,25], microwave [26–29], radio frequency [26,30], and dielectric barrier discharge [13,31–33]. Some of these studies demonstrated plasma-catalysis synergy. The basic oxides (MgO and CaO) enhanced ammonia formation, unlike acidic

oxides (Al_2O_3, WO_3, and SiO_2-Al_2O_3) [24]. The order of catalytic activity for active metals was reported as follows: Pt > stainless steel > Ag > Fe > Cu > Al > Zn in glow discharge plasma [25]. The yield of ammonia was found to be considerably enhanced by iron wires in radio frequency plasma [30].

While plasma ammonia synthesis has long been investigated, there is little data on the nature of the synergetic effect in plasma catalysis. Specifically, the influence of its chemical, physical and electrical properties on the discharge behaviour and its contribution to ammonia formation rates. In particular, the catalysts used are often impractical such as platinum metal pieces in contrast to industrially used dispersed platinum particles supported by refractory oxides. The understanding of the role of such oxide supports on plasma is a crucial step before further investigating active catalytic metals added to these support materials.

In this paper, we systematically investigate the plasma-assisted ammonia synthesis in a packed 1-sided dielectric barrier discharge (DBD) reactor. We compare the materials widely used catalyst supports for plasma-assisted ammonia syntheses and study the effect of physical properties of the material and process parameters to establish the nature of the synergetic effects in ammonia plasma-catalytic synthesis.

2 EXPERIMENTAL

2.1 Materials

Catalyst support materials were chosen based on their dielectric, physical and surface chemical properties were studied: acidic (α-Al_2O_3, TiO_2) and basic (MgO, CaO), materials with various surface area, porosity (α-Al_2O_3 and γ-Al_2O_3), and dielectric properties (quartz wool, TiO_2 and $BaTiO_3$). The following materials were purchased from Mateck GmbH in the form of ~3 mm: γ-Al_2O_3, α-Al_2O_3, TiO_2, and $BaTiO_3$. MgO and CaO were purchased in the form of lumps from Sigma Aldrich and Merck Millipore, respectively. These pellets and lumps were crushed and sieved into a series of particle fractions using a mechanical shaker. The particle sizes reported in the work are average and relate to the sieve sizes of 1600-1000, 850-630, 355-250 and 250-160 µm. The quartz wool (fibers 5-30 µm in diameter) from Carl Roth GmbH was used as purchased.

2.2 Ammonia synthesis in a DBD reactor

The plasma-assisted NH_3 synthesis was performed in a 1-sided DBD plasma reactor at an atmospheric pressure with 3 mL of the material packed in the discharge zone. The system is presented in details in reference [34] and shown schematically in Supplementary Figure S1. Briefly, a stainless steel mesh was wrapped around a quartz tube with 10 mm inner diameter and 1.5 mm thick. The mesh was a ground electrode, whereas the quartz tube served as a dielectric barrier. An axial stainless steel rod with 6 mm outer diameter was a high voltage electrode. The discharge gap was 2 mm and length of the discharge zone was 60 mm. Equations 2-4 show calculation of the total power (P_{total}), specific energy input (SEI), and the energy consumption per mole of ammonia (E_{NH3}):

$$P_{total} = f\ C_p \int_{one\ cycle} V(t)dt\ , \tag{1}$$

$$SEI = P_{tot} / Q_{gas}\ , \tag{2}$$

$$E_{NH3} = P_{tot} / (C_{NH3} \cdot Q_{gas})\ , \tag{3}$$

where, $V(t)$ is the applied voltage, C_p - capacitance of the capacitor, f - applied voltage frequency, Q_{gas} - volumetric gas flow rate, C_{NH3} – ammonia concentration in gas.

The gases (N_2, H_2, Linde Gases, 99.9%) were used as feed and their flow rate was controlled using Bronkhorst mass flow controllers. Ammonia was the only reaction product observed, in agreement with literature [31,33,35,36]. Ammonia concentration was analyzed with a Fourier transform infrared spectrophotometer (Shimadzu IRTracer-100) in a gas cell with KBr windows (Specac). The ammonia extinction coefficient was determined from a series of calibration gas mixtures. The product gases, before leaving the set-up, were scrubbed in a series of water-filled bottles to capture the ammonia produced.

The electrical power was supplied to the DBD reactor in the form of microsecond pulses (Figure S2), set by a waveform generator. The power input to DBD reactor was controlled by changing the peak to peak voltage of this pulse signal (Figure S2), which is referred to

as input voltage (V_{pk-pk}) in the manuscript. The optimum frequency and pulse width of this pulsed signal were found to be 21 kHz and 25 µs respectively, based on the highest ammonia concentration produced. Before every experiment, the DBD reactor was heated for 1 h at 150^{o}C and pre-heated nitrogen (at 150^{o}C) was flowing through the reactor at 1 L min^{-1} to dry the catalyst support. All the experiments were performed at least twice (reproducibility was above ±5%).

The temperatures of the plasma region and the gas outlet were monitored with thermocouples and an infrared (IR) camera. For monitoring the plasma region temperature, a thermocouple was placed inside the packed bed zone, so the temperature was measured immediately after plasma discharge was off. The IR camera was used to record the temperature changes for the packed bed (Figure S3 in Supplementary). The difference in the temperature recorded by the thermocouple and the IR camera was within ± 10 ^{o}C.

The maximum temperature of the packed bed zone was found to be 440 ^{o}C (see Figure S3 for effect of SEI on temperature rise within packed bed for various catalyst support materials), whereas the outgoing gaseous stream temperature was always below 23^{o}C. Under thermal catalysis conditions (at 440 ^{o}C, the highest temperature reached in this study) no ammonia formation was observed for all the materials studied.

2.3 Characterization

Surface area, the pore volume and the pore size distribution were measured by nitrogen physisorption analysis in a TriStar 3000 Micromeritrics instrument. Prior to measurement, all samples were dried at 150^{o}C for 1 h under nitrogen purging. The surface area and pore size distribution were determined using standard multipoint Brunauer-Emmett-Teller (BET) analysis and Barrett Joyner Halenda (BJH) pore distribution methods. Typical nitrogen adsorption isotherm of γ-Al_2O_3 before and after exposure to plasma is presented in Figure S4 of the Supplementary.

Scanning electron microscopy (SEM) study was performed on the Quanta 3D FEG microscope with an electron beam resolution of 1.2 nm at 30 kV and electron acceleration voltage of 0.2-30 kV. Powdered samples, as well as fractured pellets, were studied by applying them on conductive tape followed by carbon-coating before the SEM analysis.

SEM images of catalyst supports are presented in Figure S5. These characterizations were performed before and after exposure to the plasma and no appreciable differences in the catalyst supports were observed.

3 RESULTS AND DISCUSSION

The material packed into the plasma reactor can enhance the ammonia product either by improving the plasma discharge or by promoting the ammonia synthesis itself with chemical interactions. The discussion is organized firstly in discussing the effect of material on plasma; then the effect of materials on ammonia synthesis – the effect of physical and chemical properties, as well as morphology. Afterwards, we discuss the effect of process parameters on plasma-catalytic ammonia synthesis.

3.1 Effect of materials on plasma

3.1.1 Effect of material properties on plasma

Table 1 shows the main physical properties of the materials studied. These include surface area and micro-, meso- porosity which affect the possible interaction of materials with plasma dielectric constant that was reported to affect plasma generation greatly. The bandgap is a measure of electronic properties with only 2 semiconductors (TiO_2 and $BaTiO_3$) and the remaining materials being insulators. Lastly, these materials have various chemical properties – CaO and MgO are basic while Al_2O_3 and TiO_2 are acidic that was also reported to affect ammonia plasma synthesis [24].

Table 1. Properties of the support materials tested.

Support Type	Surface Area ($m^2\ g^{-1}$)	Pore size (nm)	Relative dielectric constant (-)	Bandgap (eV)
γ-Al_2O_3	111	17.1	9.3-11.5 [37]	7.6 [38]
α-Al_2O_3	0.24	5.7	9.3-11.5 [37]	7.0 [38]
TiO_2	34.1	15.9	85 [39]	3.2 [40]
MgO	0.2	9.3	9.7 [37]	6.4 [41,42]
CaO	3.5	8.9	11.8 [37]	5.7 [42]
$BaTiO_3$	0.1	11.9	400-6500 [43]	3.4 [44]
Quartz Wool	0.26	11.1	4.0 [45]	6.9 [46]
No packing (gas)	-	-	1	-

Figure 1a represents the electrical signals recorded for ammonia synthesis in the DBD reactor packed with various catalyst supports and in the empty reactor. Photographs of the plasma discharge for various catalyst supports packed in the DBD reactor are presented in Figure S6 of the Supplementary.

Discharge in the reactor reported in this study is characterized by the presence of numerous microdischarges. These microdischarges cross the gas gap and connect the cathode to the anode [47]. As can be seen from Figure 1, the voltage applied and voltage across the capacitor are quasi-sinusoidal with the increasing spikes in the capacitor voltage every half-period. These spikes (called 'ringing') in the reactor and measurement circuit indicate the presence of filamentary microdischarges. Greater ringing implies the presence of a larger number of filaments; a greater height of the spikes could imply a higher peak current per filament or superposition of overlapping ringing signals from several microdischarges occurring simultaneously.

The height and the number of spikes observed (Figure 1) depend strongly on the packing material, in agreement with literature for DBD [48]. The empty reactor (no packing) clearly demonstrates typical filamentary discharges as also reported by Mei et al. [49] and Patil et al. [34]. The addition of packing material in the discharge gap affects the discharge mode – leaving either a filamentary discharge (for moderate dielectric constant materials, Figure 1b, c, e, f, and h) or changing to a non-filamentary discharge, such as a Townsend or glow discharge (for high dielectric constant materials, Figure 1d and g). The change in the discharge mode can result in a shift in the electron energy distribution in the plasma, subsequently affecting generation of reactive species, which can then enhance the ammonia production [50].

Based on the spikes visible in the capacitor waveform in Figure 1h, the number of discharge filaments is highest for quartz wool. This may be due to the sharp edges of the quartz wool that localize filament ignition [34,49]. Similarly, packing with quartz wool can be thought of as subdividing the discharge volume into many separate small discharge gaps, for which the number of filaments increases significantly as gas gaps become thinner [48]. These effects justify the intense plasma emission observed for the reactor

packed with quartz wool (Figure S6), which is in good agreement with Patil et al. and Gallon et al. [34,51] studied for other reactions.

One of the reasons behind the difference in discharge behaviour in reactor packed with various materials could be their dielectric constants. Under the investigated experimental conditions, materials with moderate dielectric constants (such as γ-Al_2O_3, α-Al_2O_3, MgO, and CaO) show filamentary microdischarges. Materials with high dielectric constant (such as $BaTiO_3$ and TiO_2) show non-filamentary discharge [52]. A high dielectric constant of the material ensures that the applied electric field is more concentrated within the voids – more of the applied voltage drops across the gas in the voids. Since the applied voltage amplitude is the same for all packing materials in Figure 1 and Figure 2, there are greater electric field strengths across the gas when $BaTiO_3$ and TiO_2 are packed.

To make this clearer, assume a void fraction (*f)* filled with gas and fraction *(1 - f)* filled with materials with a dielectric constant ε_r. The applied voltage drops from the powered (center) electrode to the ground (outer) electrode, with a distance d between them. For simplicity, the quartz tube is neglected and a plane-parallel plate configuration is assumed. From the standard equation for plane-parallel capacitors; the capacitance of the pellets $C_{pellets}$ and the capacitance of the void fraction (or gas between the pellets) C_{gas} can be defined as in Equations 5 and 6:

$$C_{pellets} = \varepsilon_r \varepsilon_0 \frac{A}{(1-f)d}, \quad (5)$$

$$C_{gas} = \varepsilon_0 \frac{A}{fd}, \quad (6)$$

where A is the surface area of the capacitors and ε_0 is the vacuum permittivity. Since the applied voltage $V_{applied}$ drops over a distance $(1-f)d$ along the material as $\Delta V_{pellets}$ and over a distance fd along the gas as ΔV_{gas}, with $V_{applied} = \Delta V_{pellets} + \Delta V_{gas}$, the Equation 7 from circuit theory for two capacitors in series can be applied:

$$C_{pellets} \Delta V_{pellets} = C_{gas} \Delta V_{gas}, \quad (7)$$

Combining with Equations (5) and (6) gives out the difference in voltages (Equation 8):

$$\frac{\Delta V_{pellets}}{\Delta V_{gas}} = \frac{1-f}{f} \frac{1}{\varepsilon_r}. \quad (8)$$

If we now assume a void fraction f of 0.3 and a dielectric constant ε_r = 400, we find that only 0.7/(0.3·400) ≈ 0.006, or less than 1% of the applied voltage drops across the pellets and above 99% - between the pellets. The electric field resulting from the applied voltage (with an average of $V_{applied}/d$), is, therefore, mostly found in the gas between the pellets (as $\Delta V_{gas}/(fd)$).

An alternative explanation for a varying discharge behaviour of packing materials may be given by considering the electrical properties. Among the studied materials, only TiO_2 and $BaTiO_3$ are semiconductors, while other materials are insulators (see bandgaps in Table 1). Hence, the conductivity of the semiconductors might contribute towards charge homogeneity on the particle surface, thus favouring a non-filamentary discharge formation [53]. Likely, it is the combination of dielectric properties and, notably, particle shape that is responsible for the filamentary microdischarge generation.

Figure 2 shows the V-Q Lissajous figures for various materials tested at the same input voltage of 36 $V_{pk\text{-}pk}$. It can be clearly seen that the power dissipated in the reactor changes significantly depending on the type of support material packed in the DBD reactor, even though same voltage is supplied. The shape of the Lissajous figure changes from typical parallelogram to oval when $BaTiO_3$ or TiO_2 is packed in the discharge gap, in agreement with Mei et al. [49], and Butterworth and Allen [54]. The area enclosed by V-Q Lissajous figure for high dielectric materials ($BaTiO_3$ and TiO_2) is much lower than for the other materials. The power consumption in the plasma reactor is only 14.2 W for $BaTiO_3$ versus 46.6 W for γ-Al_2O_3. Quartz wool was found to be most efficient in dissipating power in the plasma discharge by generating intense filamentary discharge, as showed by the highest area enclosed in Figure 2.

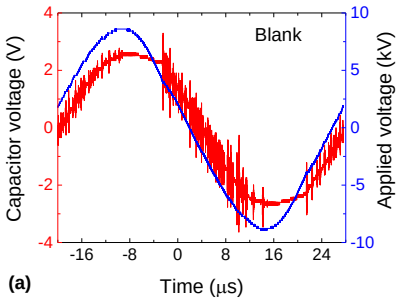
Blank
Capacitor voltage (V)
Applied voltage (kV)
Time (μs)

(a)

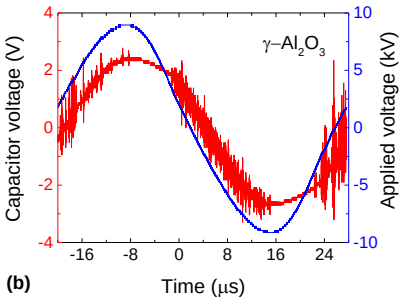
γ–Al2O3
Capacitor voltage (V)
Applied voltage (kV)
Time (μs)

(b)

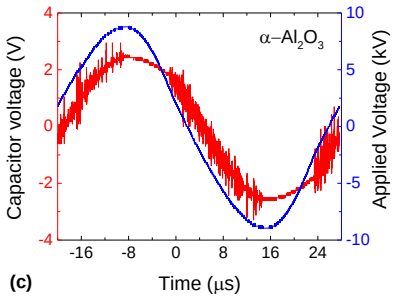
α–Al2O3
Capacitor voltage (V)
Applied Voltage (kV)
Time (μs)

(c)

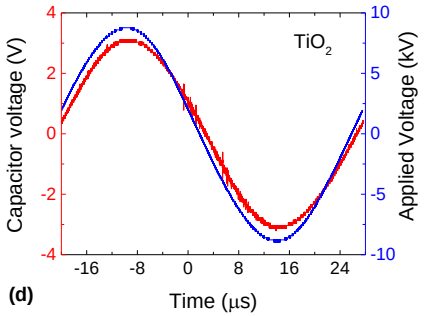
TiO2
Capacitor voltage (V)
Applied Voltage (kV)
Time (μs)

(d)

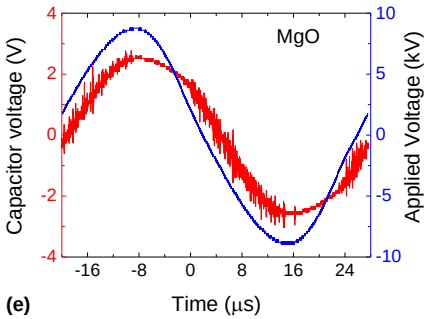
MgO
Capacitor voltage (V)
Applied Voltage (kV)
Time (μs)

(e)

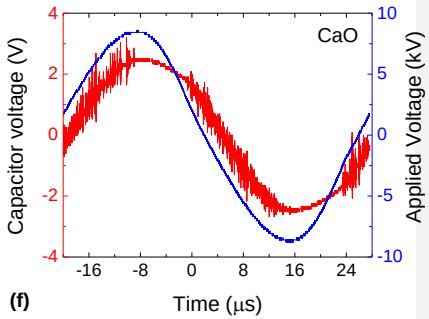
CaO
Capacitor voltage (V)
Applied Voltage (kV)
Time (μs)

(f)

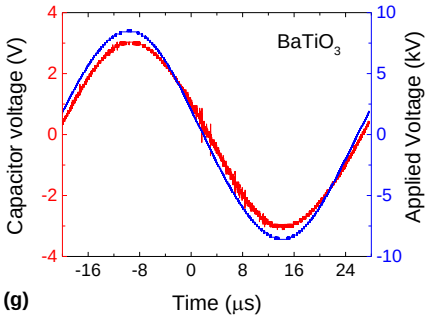
BaTiO3
Capacitor voltage (V)
Applied Voltage (kV)
Time (μs)

(g)

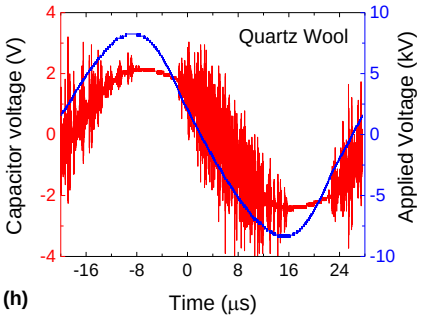
Quartz Wool
Capacitor voltage (V)
Applied Voltage (kV)
Time (μs)

(h)

Figure 1. Voltage signals in a DBD reactor packed with various materials: (a) no packing, (b) γ-Al_2O_3, (c) α-Al_2O_3, (d) TiO_2, (e) MgO, (f) CaO, (g) $BaTiO_3$, (h) Quartz wool. All materials except quartz wool are in 300 μm particles. The input voltage was 36 V_{pk-pk}, 21 kHz, pulse width of 25 μs, total gas flow rate of 0.4 L min^{-1}, N_2:H_2=0.33.

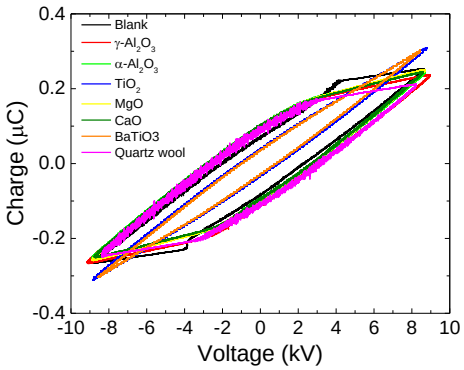

Figure 2. Lissajous figures in a DBD reactor packed with various materials. All materials except quartz wool are in 300 μm particles. The input voltage was 36 V_{pk-pk}, 21 kHz, pulse width of 25 μs, total gas flow rate of 0.4 L min^{-1}, N_2:H_2=0.33.

3.1.2 Effect of particle size on plasma

The particle size of the catalyst support also showed significant influence on the discharge characteristics. Figure 3 presents the typical electrical signals recorded for 4 different particle sizes of γ-Al_2O_3. The intensity and number of filamentary microdischarges produced in the reactor packed with particles 1300 μm (Figure 3a) and 740 μm (Figure 3b) in diameter are considerably lower than the empty DBD reactor (Figure 1a). The particle size of 300 μm (Figure 3c) has discharge behaviour similar to that of the empty reactor, but with significant changes in the ringing level during positive cycles of the applied voltage. The filamentary microdischarges produced for the smallest particle size, 200 μm (Figure 3d), are much more intense than that of the reactor without packing and that of other particle sizes investigated. Hence, smaller catalyst support particles increase density of filamentary microdischarges.

The likely reason for the effect of smaller particles onto discharges comes from the increasing porosity, number of intra-particle contacts, and lower curvature. The void fraction increases in reactors packed with the larger particles because of the wall effects [55]. Moreover, for 200 μm particles, the number of particle-particle contact points is much higher than the 1300 μm particles. The electric field strength is much higher at these contacts points [56]. Also, smaller particles have sharp edges and higher curvatures, producing higher electric field strength at these points.

The Lissajous figures are plotted for all the investigated particle sizes in Figure 4. It shows that the larger particle size fractions, 1300 and 740 µm, have a similar area enclosed on the Lissajous figure. The smallest particle size of 200 µm encloses the highest area among all particle sizes, thus indicating a higher dissipated power. The power dissipated by 1300, 740, 300 and 200 µm particle sizes are 42.2 W, 43.2 W, 46.3 W and 49.8 W, respectively at the constant input voltage of 36 V_{pk-pk}. These values are in agreement with the observed microdischarge formation behaviour in Figure 3.

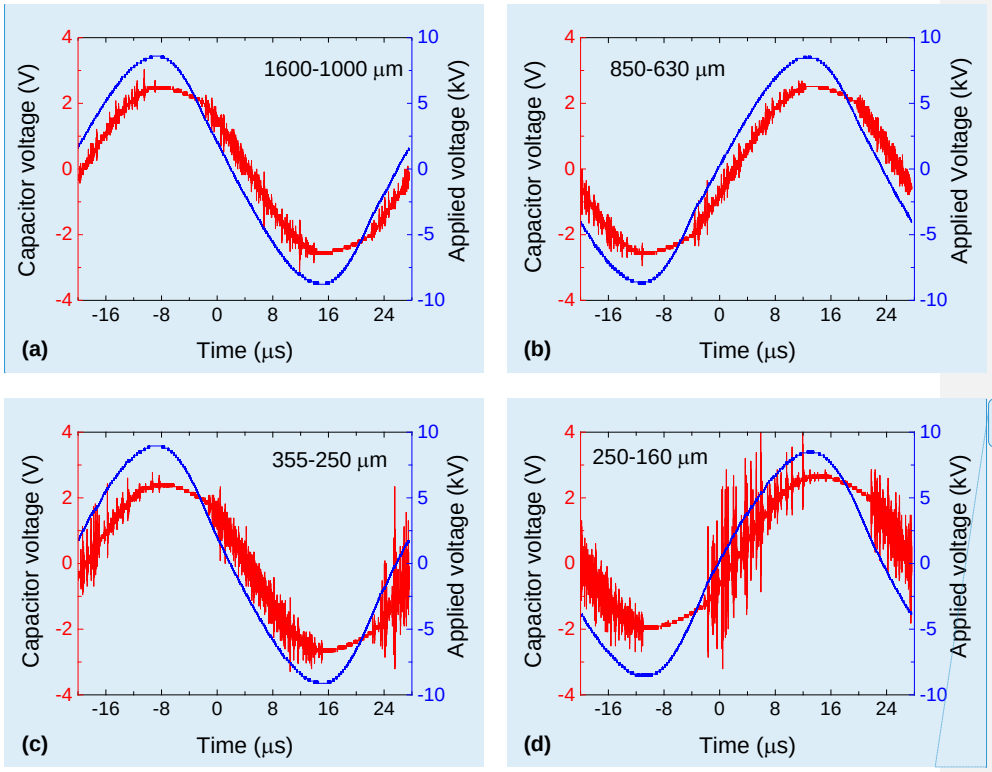

Figure 3. Electrical signals recorded for the investigated support sizes: (a) 1300 µm, (b) 740 µm, (c) 300 µm, and (d) 200 µm. The input voltage was 36 V_{pk-pk}, 21 kHz, pulse width of 25 µs, total gas flow rate of 0.4 L min^{-1}, N_2:H_2=0.33.

Commented [NC1]: Could you please put average particle sizes here instead of ranges?

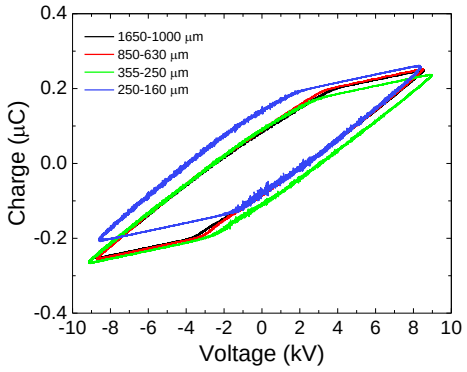

Figure 4. Lissajous figures in a DBD reactor packed with γ-Al_2O_3 particles of various average diameters. The input voltage was 36 V_{pk-pk}, 21 kHz, pulse width of 25 μs, total gas flow rate of 0.4 L min^{-1}, N_2:H_2=0.33.

When DBD is packed with any material, the average electric field strength, mean electron energy and charge transfer characteristics increase significantly [49]. Packing material in DBD reactor can be expected to increase the local electric field strength, specifically near the pellet-pellet contact points. This increase in the electric field also enhances the production of high energy electrons, which in turn initiates generation of reactive chemical species contributing to various plasma reaction channels.

3.2 Effect of materials on ammonia synthesis

3.2.1 Effect of material properties on ammonia synthesis

To investigate the influence of the various catalyst support materials on the NH_3 production, the materials with particle size 300 μm were packed in the plasma discharge zone. The concentration of ammonia was found to increase linearly with specific energy input for the empty reactor experiment and for all support materials, except for TiO_2 (Figure 5a). The slope of the concentration trend line varies with packing material; the slope is always higher than the empty reactor. The linear increase in concentration with input power has been commonly reported for plasma-assisted reactions [34,37,51]. For filamentary discharges, an increase in specific energy input results in a proportional increase in the number of filaments that are ignited in the reactor [56]. Provided each individual microdischarge produces a certain amount of ammonia, this leads to a linear relation between SEI and ammonia production. The energy consumption per mole of

ammonia (Figure 5b) increases with the specific energy input because of the concentration of ammonia does not increase exactly proportionally to SEI. For $BaTiO_3$ and TiO_2, the concentration of ammonia produced was negligible and therefore the energy consumption per mole of ammonia was high. Therefore, $BaTiO_3$ and TiO_2 are not included in Figure 5b. The lowest energy consumption per mole of ammonia produced is given by quartz wool (50.2 MJ mol^{-1} of NH_3), followed by γ-Al_2O_3 (63.2 MJ mol^{-1} of NH_3),. The quartz wool packed DBD reactor required at least 105% lower energy per mole of ammonia produced as compared to the empty reactor.

When the reactor is packed higher amounts of ammonia are produced compared to the empty reactor, except for TiO_2 and $BaTiO_3$ materials. The presence of material increases the ammonia concentration at least by 68% (for CaO). Figure 5a shows that quartz wool is the best performing packing/support material by producing 2900 ppm of ammonia, which is 113% higher than that for the blank experiment. γ-Al_2O_3 is the second best performing support, with a maximum concentration of 2660 ppm, giving 95% increase in ammonia concentration compared to the empty reactor.

Surface area and porosity do not seem to be crucial for plasma formation because α-Al_2O_3 and γ-Al_2O_3 (with similar surface properties) demonstrated almost identical ammonia formation despite an almost 100-fold different surface area. This is in line with findings of Zhang et al. [57] who showed that microdischages are formed only within pores larger than 10 μm – intraparticle voids. Plasma-activated species are unable to diffuse deep inside the nanopores of the support material due to their shore lifetime rendering the porous volume of the catalyst in plasma-catalytic reactions.

The comparison between the performance of α-Al_2O_3 and CaO, MgO shows that surface chemical properties such as acidity or basicity play a minor role in the enhancement of the ammonia production. These materials have comparable properties (Table 1) and show a similar effect on plasma formation and ammonia production.

Semiconductor materials with high dielectric constant such as $BaTiO_3$ and TiO_2 could produce only marginal amounts of ammonia (243 and 155 ppm). This low performance is explained by their ineffectiveness in producing filamentary discharges. Comparing these materials to each other, they have a close bandgap while the dielectric constant of $BaTiO_3$

is dramatically higher than that of TiO_2. However, $BaTiO_3$ shows a higher ammonia production indicating that increasing dielectric constant may improve ammonia production while a relatively low bandgap dramatically decreases it. Yet, both $BaTiO_3$ and TiO_2 were substantially inferior to other materials and to the empty reactor. The results obtained for the reactor packed with $BaTiO_3$ contrast to results obtained for CO_2 conversion by Mei et al. [49], where packing a DBD reactor with $BaTiO_3$ gave a higher conversion of CO_2.

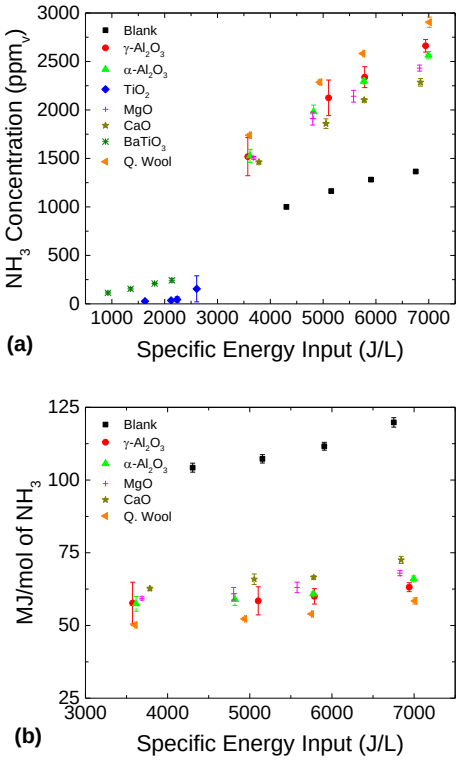

Figure 5. (a) Ammonia concentration as a function of specific energy input, (b) Energy efficiency for ammonia synthesis in a DBD reactor packed with various materials. All materials except quartz wool are in 300 µm particles. The input voltage was 36 V_{pk-pk}, 21 kHz, pulse width of 25 µs, total gas flow rate of 0.4 L min^{-1}, N_2:H_2=0.33.

There is no agreement on the effect of dielectric constant of the packing material on the discharge behaviour and the chemical reactions. Takaki et al. [58] found that dielectric

constant played no role in the C_2F_6 plasma decomposition. Similarly, Tu et al. [50,51] reported a minor influence of the packing material on breakdown voltage for dielectric constants <100. Whereas, Ogata et al. [59] found that the benzene removal efficiency increased up to the dielectric constant of 1100. These data suggest that the dielectric constant of the packing material, and the resulting discharge mode, may have varying effects for different plasma-catalytic reactions.

The catalyst supports which generate the most ringing and, therefore, likely a higher number of filamentary microdischarges, yielded a higher amount of ammonia (compare Figure 1 and Figure 5). This is in agreement with previous studies of NO_x production in DBD [34] and H_2 production in DBD [51]. When the reactor was packed with high dielectric supports (TiO_2 and $BaTiO_3$, which produce a non-filamentary discharge) almost no ammonia was formed. This suggests that the filamentary discharge is more suitable for ammonia synthesis.

3.2.2 Effect of particle size on ammonia synthesis

To investigate further the influence of the catalyst support size on the NH_3 formation, experiments were conducted with the optimum γ-Al_2O_3 material varying the particle sizes. Figure 6 shows the influence of particle size on ammonia formation and energy consumption. Smaller particles produce a higher concentration of ammonia and also consume less energy per unit mole of the product produced. The smallest particle size of 205 µm is the most energy efficient, consuming 50.8 MJ mol^{-1} of ammonia.

As discussed previously, void fraction decreases for smaller particles [55], and the number of contact points (between particle-particle, particle-dielectric and particle-electrode) increases, giving enhanced plasma discharge volume leading to increasing in power dissipation. Since this increases power consumption per unit volume of gas, the activation of the reactant molecules is also enhanced, eventually contributing to more ammonia formation. Smaller particle sizes also exhibit a higher surface to gas volume ratio, increasing both the flux of dissociated and excited plasma species to the surface and the rate of recombination reactions.

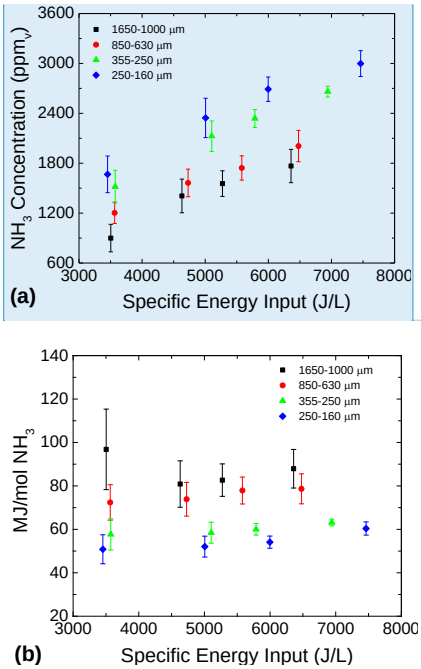

Figure 6. (a) Ammonia concentration as a function of specific energy input, (b) Energy efficiency for ammonia synthesis in a DBD reactor packed with γ-Al_2O_3 of various size. The input voltage was 36 V_{pk-pk}, 21 kHz, pulse width of 25 µs, total gas flow rate of 0.4 L min^{-1}, N_2:H_2=0.33.

As a result, smallest particle size (200 µm) have produced 64% more ammonia than the largest particle size investigated (1300 µm), when compared at the same SEI, despite a reduction in residence time due to a decrease of the void fraction.

3.3 Effect of process parameters on plasma and ammonia synthesis

3.3.1 Effect of the gas feed ratio on plasma and ammonia synthesis

The effect of feed flow ratio on NH_3 synthesis was investigated by varying the N_2/H_2 feed ratio between 0.2 and 4 in a reactor packed with γ-Al_2O_3. Figure 7 shows the effect of the feed flow ratio on ammonia concentration and energy efficiency. The concentration of ammonia keeps increasing with the flow ratio and eventually stabilizes after the flow ratio of 2.

Commented [NC2]: Could you please put average particle sizes here instead of ranges?

Surprisingly, the most commonly used stoichiometric feed ratio of 0.33 was found to produce 74% less ammonia than the feed ratio of 2. Also, the energy consumed per mole of ammonia decreased exponentially with increased in the flow ratio and stabilized at around 36 MJ mol^{-1} – 62% lower than the energy consumed at the feed ratio of 0.33.

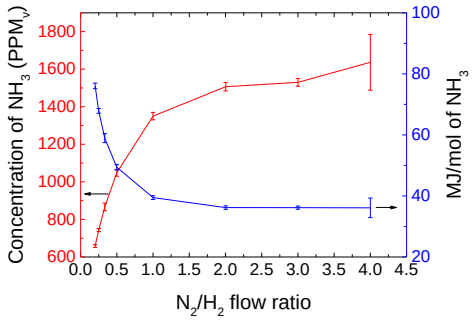

Figure 7. The effect of the gas feed ratio (N_2/H_2) on ammonia concentration and energy consumption per mole of ammonia for a DBD reactor packed with 300 µm γ-Al_2O_3 particles. The input voltage was 36 V_{pk-pk}, 21 kHz, pulse width of 25 µs, total gas flow rate of 1.0 L min^{-1}.

Excitation of nitrogen molecules is considered a rate-limiting step in plasma ammonia synthesis [60]. With the increase in the flow ratio, the amount of nitrogen in the feed increases leading to a higher amount of nitrogen being excited. According to Mizushima et al. [60], excited nitrogen species will adsorb on the surface prior to reacting with hydrogen. Moreover, ammonia could be also produced in the absence of packing material – in gas phase reactions involving excited nitrogen species. In that case, increasing the nitrogen content also increases the probability of nitrogen excitation in plasma leading to an improved ammonia production.

The applied and capacitor voltage (Figure S7 of the Supplementary) also show that the number of intense microdischarges increases with the feed ratio. Hence, increasing nitrogen content in gas phase also facilitates formation of plasma further contributing to enhanced ammonia synthesis observed in the experiments.

3.3.2 Effect of total flow rate on plasma and ammonia synthesis

The total flow rate determines the residence time in the reactor. Ammonia plasma synthesis was investigated for at various flow rates in the reactor packed with γ-Al_2O_3 particles. The Lissajous measurements were not affected by the flow rate, implying that the discharge behaviour is not influenced by the increase in flow rates (Figure S8). The flow rates of 0.4, 1.0 and 1.5 L min^{-1} provide average residence times of 136, 54, and 36 ms. The residence time in an empty reactor at a flow rate of 0.4 L min^{-1} was 450 ms.

Figure 8 depicts the effect of a change in feed flow rate and SEI on ammonia production and energy consumed per mole of ammonia. The ammonia concentration increases proportionally to specific energy input for all the flow rates investigated. However, the ammonia concentration does not depend strongly on the flow rate. Comparing the ammonia production at the flow rates of 1.5 L min^{-1} and 1.0 L min^{-1} at the same SEI, a factor 1.5 increase in residence time increases the ammonia concentration by only 10-20%.

Figure 8b shows the energy consumption per mole of ammonia for the various flow rates. Contrary to Figure 5b where the N_2/H_2 ratio was 0.33, compared to 2.0 used here, the energy consumption increases with increase in the SEI. A flow rate of 1 L min^{-1} consumed the lowest energy per mole of ammonia of 27.9 MJ mol^{-1} (1.9 g kWh^{-1}), however, the concentration of ammonia was only 1000 ppm.

Commented [NC3]: Could you please check if Figure 8b is correct

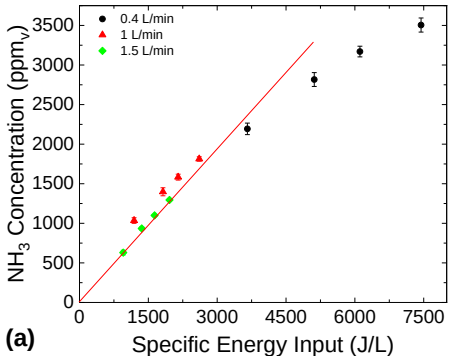

(a)

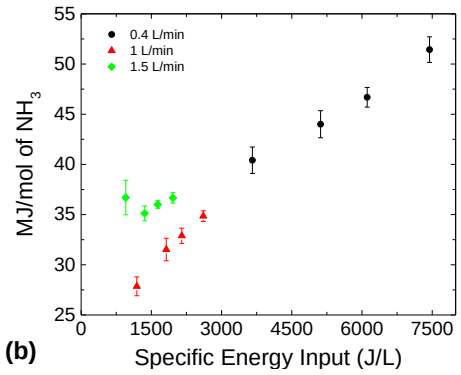

Figure 8. Effect of flow rate on (a) ammonia concentration and (b) energy consumption per mole of ammonia for a DBD reactor packed with 300 µm γ-Al_2O_3 particles. The input voltage was 36 V_{pk-pk}, 21 kHz, pulse width of 25 µs, total gas flow rate of 0.4 L min^{-1}, N_2:H_2=2.0.

We achieved the highest ammonia concentration of 3505 ppm at the flow rate of 0.4 L min^{-1} yielding an energy consumption of 51.4 MJ mol^{-1}. Per pass conversion of nitrogen was approximately only 0.26%. For a lower per pass conversion at 1 L min^{-1}, the energy consumption is found to be as low as 27.4 MJ mol^{-1}. Gomez-Ramirez et al. [61] have obtained slightly worse energy efficiency of 68.1 MJ mol^{-1}, which is 37% lower than the one achieved in this study. Bai et al. [31] have reported a better energy efficiency of 33.5 MJ mol^{-1} in a micro-DBD reactor. Gomez-Ramirez et al. [61] and Hong et al. [62] have reported a higher per pass conversions of nitrogen of 1.83% and 0.57% at a much higher residence time of 17.5 s and 30 s, respectively. These higher residence times are achieved by using significantly lower flow rates, which result in more power input per litre of gas passed through the system, hence higher SEI.

3.3.3 Effect of argon addition on plasma and ammonia synthesis

The effect of the flow feed ratio shows that the addition of nitrogen into the gas stream (Figure 7) facilitates plasma formation. Argon was reported to enhance the ammonia formation, because of a more uniform and intense plasma discharge formation [62]. An experiment was conducted to investigate the effect of argon addition to study the effect of argon.

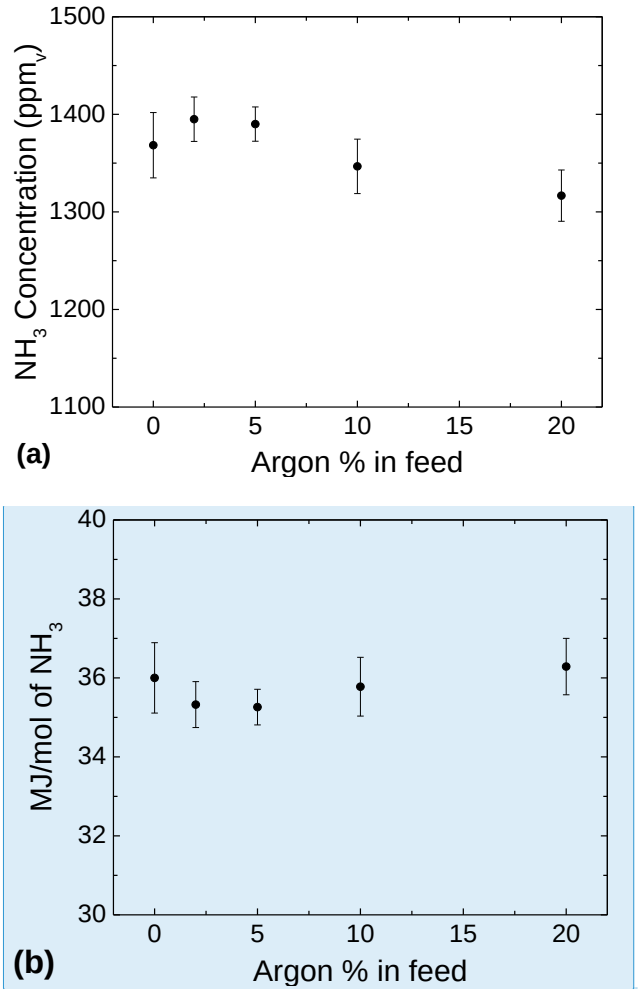

Commented [NC4]: Could you combine these 2 figures into one with 2 Y axes – similar to Fig 7 ?

Figure 9. Effect of argon addition in to the feed gas for a DBD reactor packed with 300 µm γ-Al_2O_3 particles. The input voltage was 36 V_{pk-pk}, 21 kHz, pulse width of 25 µs, total gas flow rate of 0.4 L min^{-1}, N_2:H_2=2.0.

When argon is added to the feed (Figure 9), the ammonia production goes through a maximum at the concentration between 2 vol% and 5 vol%. A further increase in argon concentration results in the ammonia concentration decline by 5.6%. This could be

explained by the decrease in the dissipated power in the discharge zone at higher argon content (Figure S9), which falls 3.2% from 33.9 W to 32.8 W. The fact that the ammonia concentration drop is higher than the drop in power can be attributed to the dilution of the reactive gases (N_2 and H_2) resulting in the lower probability of their activation.

A dilution by 20 vol% with argon leads to only a few percent decline in ammonia production – this suggests that argon does have a beneficial effect on the reaction chemistry. The addition of argon encourages the formation of excited nitrogen species by charge transfer between Ar^+ and N_2 [63]. The subsequent interactions of excited nitrogen species with hydrogen increase ammonia formation.

The addition of 2 vol% argon increases the ammonia concentration by 2% and reduces energy efficiency of ammonia production. However, adding argon to the reactant gases also brings practical challenges for the separation of product and reactant gases. As a result, the cost and energy required is likely higher than the gains made in the energy efficiency and ammonia concentration in the reactor section, thus it may not be beneficial in practical applications.

4 CONCLUSIONS

We have performed a systematic study on plasma-assisted ammonia synthesis using a range of materials commonly used catalyst supports: γ-Al_2O_3, α-Al_2O_3, MgO, CaO, quartz wool, TiO_2, and $BaTiO_3$. All the support materials excluding the last 2 showed a strong synergetic effect – the amount of ammonia formed exceeded the sum observed without plasma, or in plasma without any material packed into the reactor.

The quartz wool and γ-Al_2O_3 produced the highest amount of ammonia, yielding an additional 113% and 95% of NH_3, respectively, compared to an empty reactor. The effect was caused by (i) the enhanced plasma generation and a higher production of excited species in the plasma, and (ii) by an increased in the available intra-particle surface area.

A comparison of physical and chemical properties of the materials shows that micro- and meso- porosity and associated surface area of the material plays no role in plasma catalysis. Basic and acidic surface properties did not also affect the reaction. High dielectric constant and a relatively low bandgap (semiconductor materials) reduced

plasma generation and hindered ammonia formation. Non-filamentary discharges prevailed for materials with high dielectric constants (TiO_2 and $BaTiO_3$).

Filamentary microdischarges generated by other materials, on the contrary, enhanced ammonia production. These microdischarges are facilitated by materials with smaller the particle sizes. The smallest investigated particle size of γ-Al_2O_3, 200 µm, produced 2990 ppm of ammonia at the energy consumption of 60 MJ mol^{-1} – 64% higher concentration and 30% lower energy compared to particles 1300 µm in diameter.

The process parameters also notably affect the plasma generation. The N_2/H_2 feed ratio greater than 2 gives 74% higher ammonia concentrations of NH_3 and improves energy efficiency compared to the stoichiometric feed ratio of 0.33. This reveals that the excitation and/or dissociation of nitrogen is the rate limiting step. The residence time has minor effect on plasma ammonia formation likely because the intrinsic time of plasma processes (~1 ms – 1 µs) is substantially smaller than residence time studies (~100 ms). Addition of argon (2-5 vol%) to the feed increases ammonia concentration on an average by 2% in terms of concentration and energy efficiency. A dilution of the feed gas by 20% of argon only reduced ammonia production by only 5.6%, which indicates that nitrogen excitation benefits from charge transfer from excited argon species.

5 ACKNOWLEDGEMENT

This research is funded by the EU project MAPSYN: Microwave, Acoustic and Plasma SYNtheses, under the grant agreement no. CP-IP 309376 in the European Community's Seventh Framework Program.

6 REFERENCES

[1] M. Appl, Ammonia, 2. Production Processes, Ullmann's Encycl. Ind. Chem. (2012) 139–225. doi:10.1002/14356007.o02.

[2] B.S. Patil, V. Hessel, L.C. Seefeldt, D.R. Dean, B.M. Hoffman, B.J. Cook, L.J. Murray, Nitrogen Fixation, in: Ullmann's Encycl. Ind. Chem., Wiley-VCH Verlag GmbH & Co. KGaA, Weinheim, Germany, 2017: pp. 1–21. doi:10.1002/14356007.a17_471.pub2.

[3] V. Smil, Enriching the Earth: Fritz Haber, Carl Bosch, and the Transformation of World Food Production, MIT Press, 2004. http://books.google.com/books?hl=en&lr=&id=G9FljcEASycC&pgis=1 (accessed June 28, 2014).

[4] M. Appl, The Haber-Bosch Heritage: The Ammonia Production Technology, in: 50th Anniv. IFA Tech. Conf., 1997: p. 25.

[5] R.R. Schrock, Reduction of dinitrogen, Proc. Natl. Acad. Sci. U. S. A. 103 (2006) 17087. doi:10.1073/pnas.0603633103.

[6] I. Rafiqul, C. Weber, B. Lehmann, A. Voss, Energy efficiency improvements in ammonia production - Perspectives and uncertainties, Energy. 30 (2005) 2487–2504. doi:10.1016/j.energy.2004.12.004.

[7] J. Gieshoff, J. Lang, Process For The Plasma-Catalytic Production of Ammonia, US6471932, 2002.

[8] E. Morgan, J. Manwell, J. McGowan, Wind-powered ammonia fuel production for remote islands: A case study, Renew. Energy. 72 (2014) 51–61. doi:10.1016/j.renene.2014.06.034.

[9] R. Lan, J.T.S. Irvine, S. Tao, Ammonia and related chemicals as potential indirect hydrogen storage materials, Int. J. Hydrogen Energy. 37 (2012) 1482–1494. doi:10.1016/j.ijhydene.2011.10.004.

[10] S. Samukawa, M. Hori, S. Rauf, K. Tachibana, P. Bruggeman, G. Kroesen, J.C. Whitehead, A.B. Murphy, A.F. Gutsol, S. Starikovskaia, U. Kortshagen, J.-P. Boeuf,

T.J. Sommerer, M.J. Kushner, U. Czarnetzki, N. Mason, The 2012 Plasma Roadmap, J. Phys. D. Appl. Phys. 45 (2012) 253001. doi:10.1088/0022-3727/45/25/253001.

[11] R. Ingels, D. Graves, S. Anderson, R. Koller, Modern Plasma Technology for Nitrogen Fixation: New Opportunities?, in: Mod. Plasma Technol. Nitrogen Fixat. New Oppor., International Fertiliser Society, London, UK, 2015: pp. 1–27.

[12] N. Cherkasov, A.O. Ibhadon, P. Fitzpatrick, A review of the existing and alternative methods for greener nitrogen fixation, Chem. Eng. Process. Process Intensif. 90 (2015) 24–33. doi:10.1016/j.cep.2015.02.004.

[13] B.S. Patil, Plasma (Catalyst) – Assisted Nitrogen Fixation : Reactor Development for Nitric Oxide and Ammonia Production, Technische Universiteit Eindhoven, 2017. https://pure.tue.nl/ws/files/64000562/20170510_Patil.pdf.

[14] B.S. Patil, J. Rovira Palau, V. Hessel, J. Lang, Q.Wang, Q. Wang, Plasma Nitrogen Oxides Synthesis in a Milli-scale Gliding Arc reactor: Investigating the electrical and process parameters., Plasma Chem. Plasma Process. Accepted (2015) 241–257. doi:10.1007/s11090-015-9671-4.

[15] B.S. Patil, F.J.J. Peeters, G.J. van Rooij, J.A. Medrano, F. Gallucci, J. Lang, Q. Wang, V. Hessel, Plasma assisted nitrogen oxide production from air: Using pulsed powered gliding arc reactor for a containerized plant, AIChE J. 64 (2018) 526–537. doi:10.1002/aic.15922.

[16] W. Wang, B.S. Patil, S. Heijkers, V. Hessel, A. Bogaerts, Nitrogen fixation by gliding arc plasma: Better insight by chemical kinetics modeling, ChemSusChem. 10 (2017) 2145–2157. doi:10.1002/cssc.201700095.

[17] A. Fridman, Plasma Chemistry, Cambridge University Press, New York, 2008.

[18] M.A. Lieberman, A.J. Lichtenberg, Principles of Plasma Discharges and Materials Processing, Wiley, 2005.

[19] A.A.O. Catalyst, C.E. Stere, W. Adress, R. Burch, S. Chansai, A. Goguet, W.G. Graham, F. De Rosa, V. Palma, C. Hardacre, Ambient Temperature Hydrocarbon

Selective Catalytic Reduction of NO x Using Atmospheric Pressure Nonthermal Plasma Activation of a, (2014).

[20] A. Gómez-Ramírez, V.J. Rico, J. Cotrino, A.R. González-Elipe, R.M. Lambert, Low temperature production of formaldehyde from carbon dioxide and ethane by plasma-Assisted catalysis in a ferroelectrically moderated dielectric barrier discharge reactor, ACS Catal. 4 (2014) 402–408. doi:10.1021/cs4008528.

[21] L. Wang, Y. Yi, Y. Zhao, R. Zhang, J. Zhang, H. Guo, NH3 Decomposition for H2 Generation: Effects of Cheap Metals and Supports on Plasma–Catalyst Synergy, ACS Catal. (2015) 4167–4174. doi:10.1021/acscatal.5b00728.

[22] E.C. Neyts, a Bogaerts, Understanding plasma catalysis through modelling and simulation—a review, J. Phys. D. Appl. Phys. 47 (2014) 224010. doi:10.1088/0022-3727/47/22/224010.

[23] E.C. Neyts, K. (Ken) Ostrikov, M.K. Sunkara, A. Bogaerts, Plasma Catalysis: Synergistic Effects at the Nanoscale, Chem. Rev. 115 (2015) 13408–13446. doi:10.1021/acs.chemrev.5b00362.

[24] K. Sugiyama, K. Akazawa, M. Oshima, H. Miura, T. Matsuda, O. Nomura, Ammonia Synthesis by Means of Plasma over MgO Catalyst, Plasma Chem. Plasma Process. 6 (1986) 179–193.

[25] K.S. Yin, M. Venugopalan, Plasma chemical synthesis. I. Effect of electrode material on the synthesis of ammonia, Plasma Chem. Plasma Process. 3 (1983) 343–350.

[26] H. Uyama, O. Matsumoto, Synthesis of ammonia in high-frequency discharges, Plasma Chem. Plasma Process. 9 (1989) 13–24. doi:10.1007/BF01015824.

[27] H. Uyama, O. Matsumoto, Synthesis of ammonia in high-frequency discharges. II. Synthesis of ammonia in a microwave discharge under various conditions, Plasma Chem. Plasma Process. 9 (1989) 421–432. http://link.springer.com/article/10.1007/BF01083676 (accessed June 12, 2013).

[28] S. Tanaka, H. Uyama, O. Matsumoto, Synergistic effects of catalysts and plasmas

on the synthesis of ammonia and hydrazine, Plasma Chem. Plasma Process. 14 (1994) 491–504. http://link.springer.com/article/10.1007/BF01570208 (accessed December 16, 2013).

[29] J. Nakajima, H. Sekiguchi, Synthesis of ammonia using microwave discharge at atmospheric pressure, Thin Solid Films. 516 (2008) 4446–4451. doi:10.1016/j.tsf.2007.10.053.

[30] H. Uyama, T. Nakamura, S. Tanaka, O. Matsumoto, Catalytic effect of iron wires on the syntheses of ammonia and hydrazine in a radio-frequency discharge, Plasma Chem. Plasma Process. 13 (1993) 117–131. doi:10.1007/BF01447174.

[31] M. Bai, Z. Zhang, X. Bai, M. Bai, W. Ning, Plasma synthesis of ammonia with a microgap dielectric barrier discharge at ambient pressure, IEEE Trans. Plasma Sci. 31 (2003) 1285–1291. doi:10.1109/TPS.2003.818761.

[32] M. Bai, Z. Zhang, M. Bai, X. Bai, H. Gao, Synthesis of Ammonia Using CH4/N2 Plasmas Based on Micro-Gap Discharge under Environmentally Friendly Condition, Plasma Chem. Plasma Process. 28 (2008) 405–414. doi:10.1007/s11090-008-9132-4.

[33] T. Mizushima, K. Matsumoto, J. Sugoh, H. Ohkita, N. Kakuta, Tubular membrane-like catalyst for reactor with dielectric-barrier-discharge plasma and its performance in ammonia synthesis, Appl. Catal. A Gen. 265 (2004) 53–59. doi:10.1016/j.apcata.2004.01.002.

[34] B.S. Patil, N. Cherkasov, J. Lang, A.O. Ibhadon, V. Hessel, Q. Wang, Low temperature plasma-catalytic NO x synthesis in a packed DBD reactor : Effect of support materials and supported active metal oxides, Appl. Catal. B Environ. 194 (2016) 123–133. doi:10.1016/j.apcatb.2016.04.055.

[35] G. Akay, K. Zhang, Process Intensification in Ammonia Synthesis Using Novel Coassembled Supported Microporous Catalysts Promoted by Nonthermal Plasma, Ind. Eng. Chem. Res. 56 (2017) 457–468. doi:10.1021/acs.iecr.6b02053.

[36] B. Mingdong, B. Xiyao, Z. Zhitao, Synthesis of Ammonia in a Strong Electric Field Discharge at Ambient Pressure, Plasma Chem. Plasma Process. 20 (2000) 511–

520.

[37] X. Duan, Z. Hu, Y. Li, B. Wang, Effect of Dielectric Packing Materials on the Decomposition of Carbon Dioxide Using DBD Microplasma Reactor, AIChE J. (2014). doi:10.1002/aic.

[38] E.O. Filatova, A.S. Konashuk, Interpretation of the Changing the Band Gap of Al2O3 Depending on Its Crystalline Form: Connection with Different Local Symmetries, J. Phys. Chem. C. 119 (2015) 20755–20761. doi:10.1021/acs.jpcc.5b06843.

[39] A. Materials, Titanium Dioxide Titania (TiO2), (2002) 2–5.

[40] Y. Chimupala, R. Simpson, R. Mitchell, R. Douthwaite, S.J. Milne, R.D. Brydson, Synthesis and characterization of mixed phase anatase TiO2 and sodium-doped TiO2(B) thin films by low pressure chemical vapour deposition (LPCVD), RSC Adv. 4 (2014) 48507–48515. doi:10.1039/C4RA07570F.

[41] S. Heo, E. Cho, H. Lee, G.S. Park, H.J. Kang, T. Nagatomi, P. Choi, B. Choi, Band gap and defect states of MgO thin films investigated using reflection electron energy loss spectroscopy, AIP Adv. 5 (2015) 1–8. doi:10.1063/1.4927547.

[42] J.A. Mcleod, R.G. Wilks, N.A. Skorikov, L.D. Finkelstein, E.Z. Kurmaev, A. Moewes, Band gaps and electronic structure of alkaline-earth and post-transition-metal oxides, Phys. Rev. B. 81 (2010) 1–9. doi:10.1103/PhysRevB.81.245123.

[43] B. Huybrechts, K. Ishizaki, M. Takata, The positive temperature coefficient of resistivity in barium titanate, J. Mater. Sci. 30 (1995) 2463–2474. doi:10.1007/BF00362121.

[44] F.M. Michel-Calendini, G. Mesnard, Band structure and optical properties of tetragonal BaTiO3, J. Phys. C Solid State Phys. 6 (1973) 1709–1722.

[45] U. Jeckel, S. Hildebrandt, Quartz Wool Specifications, Carl Roth. (2017).

[46] E. Calabrese, W.B. Fowler, Electronic energy-band structure of a quartz, Phys. Rev. B. 18 (1978) 2888–2896.

[47] V.I. Gibalov, G.J. Pietsch, Dynamics of dielectric barrier discharges in different

arrangements, Plasma Sources Sci. Technol. 21 (2012) 024010. doi:10.1088/0963-0252/21/2/024010.

[48] F. Peeters, The Electrical Dynamics of Dielectric Barrier Discharges, Eindhoven University of Technology, Eindhoven, The Netherlands, 2015.

[49] D. Mei, X. Zhu, Y.-L. He, J.D. Yan, X. Tu, Plasma-assisted conversion of CO 2 in a dielectric barrier discharge reactor: understanding the effect of packing materials, Plasma Sources Sci. Technol. 24 (2015) 015011. doi:10.1088/0963-0252/24/1/015011.

[50] X. Tu, H.J. Gallon, J.C. Whitehead, Electrical and spectroscopic diagnostics of a single-stage plasma-catalysis system: effect of packing with TiO 2, J. Phys. D. Appl. Phys. 44 (2011) 482003. doi:10.1088/0022-3727/44/48/482003.

[51] H.J. Gallon, X. Tu, J.C. Whitehead, Effects of Reactor Packing Materials on H2 Production by CO2 Reforming of CH4 in a Dielectric Barrier Discharge, Plasma Process. Polym. 9 (2012) 90–97. doi:10.1002/ppap.201100130.

[52] N. Naudé, J.-P. Cambronne, N. Gherardi, F. Massines, Electrical model and analysis of the transition from an atmospheric pressure Townsend discharge to a filamentary discharge, J. Phys. D. Appl. Phys. 38 (2005) 530–538. doi:10.1088/0022-3727/38/4/004.

[53] Y.B. Golubovskii, V.A. Maiorov, P. Li, M. Lindmayer, Effect of the barrier material in a Townsend barrier discharge in nitrogen at atmospheric pressure, J. Phys. D. Appl. Phys. 39 (2006) 1574.

[54] T. Butterworth, R. Elder, R. Allen, Effects of particle size on CO2 reduction and discharge characteristics in a packed bed plasma reactor, Chem. Eng. J. 293 (2016) 55–67. doi:10.1016/j.cej.2016.02.047.

[55] F. Benyahia, K.E. O'Neill, Enhanced voidage correlations for packed beds of various particle shapes and sizes, Part. Sci. Technol. 23 (2005) 169–177. doi:10.1080/02726350590922242.

[56] W.S. Kang, J.M. Park, Y. Kim, S.H. Hong, Numerical study on influences of barrier

arrangements on dielectric barrier discharge characteristics, IEEE Trans. Plasma Sci. 31 (2003) 504–510. doi:10.1109/TPS.2003.815469.

[57] Y.-R. Zhang, K. Van Laer, E.C. Neyts, A. Bogaerts, Can plasma be formed in catalyst pores? A modeling investigation, Appl. Catal. B Environ. 185 (2016) 56–67. doi:10.1016/j.apcatb.2015.12.009.

[58] K. Takaki, K. Urashima, J.S. Chang, Ferro-electric pellet shape effect on C2F6 removal by a packed-bed-type nonthermal plasma reactor, IEEE Trans. Plasma Sci. 32 (2004) 2175–2183. doi:10.1109/TPS.2004.837614.

[59] A. Ogata, N. Shintani, K. Mizuno, S. Kushiyama, T. Yamamoto, Decomposition of benzene using a nonthermal plasma reactor packed with ferroelectric pellets, IEEE Trans. Ind. Appl. 35 (1999) 753–759. doi:10.1109/28.777181.

[60] T. Mizushima, K. Matsumoto, H. Ohkita, N. Kakuta, Catalytic Effects of Metal-loaded Membrane-like Alumina Tubes on Ammonia Synthesis in Atmospheric Pressure Plasma by Dielectric Barrier Discharge, Plasma Chem. Plasma Process. 27 (2006) 1–11. doi:10.1007/s11090-006-9034-2.

[61] A. Gómez-Ramírez, J. Cotrino, R.M. Lambert, A.R. González-Elipe, Efficient synthesis of ammonia from N2 and H2 alone in a ferroelectric packed-bed DBD reactor, Plasma Sources Sci. Technol. 24 (2015) 065011. doi:10.1088/0963-0252/24/6/065011.

[62] J. Hong, S. Prawer, A.B. Murphy, Production of Ammonia by Heterogeneous Catalysis in a Packed-Bed Dielectric-Barrier Discharge : Influence of Argon Addition and Voltage, IEEE Trans. PLASMA Sci. 42 (2014) 2338–2339.

[63] E. Carrasco, M. Jiménez-Redondo, I. Tanarro, V.J. Herrero, Neutral and ion chemistry in low pressure dc plasmas of H2/N2 mixtures: routes for the efficient production of NH3 and NH4(+)., Phys. Chem. Chem. Phys. 13 (2011) 19561–72. doi:10.1039/c1cp22284h.